JPEDAV (2006) 27:644-650
DOI: 10.1361/154770306X153684
1547-7037/$19.00 ©ASM International

Adsorption and Desorption of Oxygen at Metal-Oxide Interfaces: Two-Dimensional Modeling Approaches

A. Öchsner, M. Stasiek, and J. Grácio

(Submitted March 27, 2006; in revised form May 23, 2006)

A numerical approach is presented for the segregation of atomic oxygen at Ag-MgO interfaces for a system of MgO particles dispersed in an Ag matrix. General segregation kinetics is considered, and the coupled system of partial differential equations is solved using a two-dimensional finite element scheme. An indirect integration procedure for the oxygen surface coverage has been implemented into a commercial code. This numerical approach allows for the consideration of general boundary conditions, specimen sizes, and time- or concentration-dependent material and process parameters. The method is applied to periodic and stochastic model oxide distributions.

Keywords finite element method, mathematical modeling, numerical modeling, segregation

1. Introduction

Metal-ceramic phase boundaries are of great importance for many applications in materials science technology,[1,2] for example, to thin solid films, coatings, electronic packaging, supported catalysts, and fiber-reinforced metal-matrix composites. In many dispersion-hardened alloys (e.g., silver, copper, and nickel), metal/oxide interfaces are involved in strengthening mechanisms. They are also included in microminiature electronic devices, for example, metal-oxide-semiconductor field-effect transistors (MOSFET). A useful technique to produce fine oxide particles uniformly dispersed in a metallic matrix is the internal oxidation of alloys.[3] Silver is one of the favorite base materials for internal oxidation experiments.[4-6] This special status stems from practical reasons[7] since small volume fractions of an alloying addition (e.g., Al, Mg, . . .), which forms the dispersed particles, result in significant hardening effects.

This article was presented at the Multicomponent-Multiphase Diffusion Symposium in Honor of Mysore A. Dayananda, which was held during TMS 2006, 135th Annual Meeting and Exhibition, March 12-16, 2006, in San Antonio, TX. The symposium was organized by Yongho Sohn of University of Central Florida, Carelyn E. Campbell of National Institute of Standards and Technology, Richard D. Sisson, Jr., of Worcester Polytechnic Institute, and John E. Morral of Ohio State University.

A. Öchsner and **J. Grácio,** Centre for Mechanical Technology and Automation, University of Aveiro and Department of Mechanical Engineering, University of Aveiro, Campus Universitário de Santiago, 3810-193 Aveiro, Portugal; and **M. Stasiek,** Centre for Mechanical Technology and Automation, University of Aveiro Campus Universitário de Santiago, 3810-193 Aveiro, Portugal. Contact e-mail: aoechsner@mec.ua.pt.

The presence of solute atoms at internal metal/oxide interfaces influences the physical properties of the interfaces and this, in turn, may affect the bulk properties.[8] Therefore, it is important to accurately predict and measure the level of solute-atom segregation at internal interfaces. In recent papers,[9,10] the segregation of oxygen to metal/oxide interfaces has been numerically investigated based on one-dimensional finite difference models and the influence of various effects such as kinetic order or nonhomogeneity of the oxide distributions were investigated. Although several strategies for the conversion of two- or three-dimensional microstructures into representative one-dimensional distributions has been proposed (e.g., Ref 11), the demand for high accuracy necessitates the development of procedures that allow for the consideration of real particle distributions and shapes without major simplifications.

In the present work, an AgMg-alloy is considered where small precipitates of MgO were formed by internal oxidation within the Ag matrix. This system is considered as a useful model for the basic understanding of metal/oxide interfaces.[12] The segregation of oxygen at Ag/MgO interfaces is numerically simulated based on the finite element method. The presented simulations are related to a state after the formation of oxide particles; that is, the internal oxidation itself is not considered within the computational model. A schematic sketch of the physical problem is shown in Fig. 1. The use of a commercial finite element code reveals the advantage that even complex geometries and particle distributions can easily be integrated in the simulation. To process the coupled system of partial differential equations, the functionality of the code has been extended via special subroutines.

2. General Kinetics of Segregation

The kinetics of oxygen segregation at metal/oxide interfaces can be described based on Fick's second law of diffusion for the oxygen mole fraction ψ_O as:

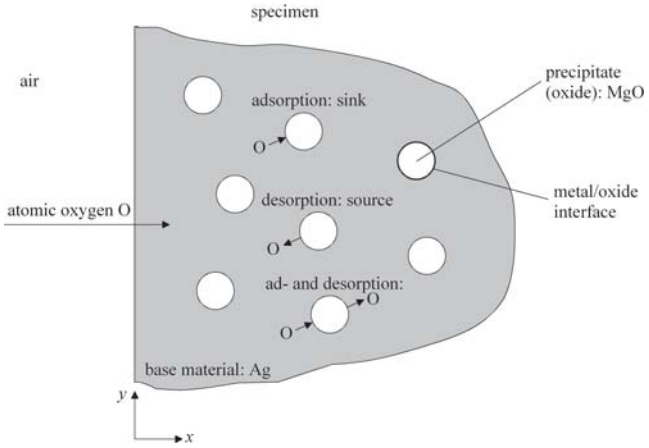

Fig. 1 Schematic description of the problem

$$\frac{\partial \psi_O}{\partial t} = \mathrm{div}(D_O \, \mathrm{grad}\psi_O) + c \cdot \gamma_O \qquad \text{(Eq 1)}$$

where D_O denotes the diffusion coefficient of oxygen in the alloy and div and grad are the divergence and gradient operator, respectively. The general source expression γ_O[13,14] involves adsorption (index a) and desorption (index d) at time t as:

$$\gamma_O/(n_{max} \cdot A) = (1-\Theta)^{\alpha} \cdot \psi_O \cdot \nu_a \exp\left(-\frac{E_a}{RT}\right)\exp\left(-\frac{a\Theta}{RT}\right) - \Theta^{\beta} \cdot \nu_d \exp\left(-\frac{E_d}{RT}\right)\exp\left(\frac{b\Theta}{RT}\right) = \frac{\partial \Theta}{\partial t} \qquad \text{(Eq 2)}$$

where the oxygen surface coverage Θ is the fraction between the actual amount of segregated oxygen atoms at the metal/oxide interface and the maximum possible amount ($0 \leq \Theta \leq 1$).

Constants α and β denote the kinetic order and ν the frequency of the adsorption and desorption process,[14] n_{max} is the maximum amount of segregation sites per area and A the surface area of the metal/oxide interfaces. It is important for the numerical approach to underline that the general source expression given in Eq 2 depends not only on Θ but also on the oxygen mole fraction ψ_O and that Eq 1 and 2 constitute a coupled system of partial differential equations. In Eq 1, the material depending factor $c = M_{tot}/(N_A \cdot \rho_{tot} \cdot V_{tot})$, where M is the molar mass, ρ is the mass density, and V is the volume of the entire specimen that is composed of the base material and the oxide (index "tot"). In a first approximation, the molar mass and the mass density of the base material can be taken as the total values because the content of the alloying addition is very small. N_A is Avogadro's constant and has been introduced to ensure unit consistency for the general source expression γ_O: Equation 1 has the unit $(\mathrm{mole_O/mole_{tot}})/\mathrm{s}$ while γ_O has the unit particles/s.

It should be noted here that the counter diffusion of the alloying addition (Mg) in a direction to the penetrating oxygen has been neglected within the authors' numerical studies. This assumption holds for many systems since the diffusion coefficient of the alloying addition is normally some orders smaller than the diffusion coefficient of oxygen in the base material. Additionally, effects arising from the change of the particle size, for example, a changing mechanical stress field, are here neglected and reserved for coupled mechanical-diffusive analysis. A final assumption for the numerical calculation is related to the oxygen coverage: once a monolayer of oxygen is formed, that is, oxygen coverage equal to one, no more oxygen atom can be attached on the oxide surface.

3. Finite Element Approach

The basic idea of the finite element method is the decomposition of a domain with an arbitrary geometry into geometrically simple elements, such that the governing differential equations can be satisfied in an average sense over these finite elements. The single elements are then assembled to obtain the complete system solution using given boundary conditions. The assembly process uses appropriate balance equations at the nodes that are used to define the elements and serve as connection points between the elements. Compared with other numerical approximate methods, for example, boundary and finite difference method, the finite element method can be regarded as the standard simulation tool in industrial practice, possessing the advantage that arbitrary geometries and any kind of nonlinearities can be easily considered. Many commercial codes are available and reveal the advantage that they comprise powerful components such as equation solvers or pre- and postprocessors. Therefore, the authors prefer to take advantage of the specialized and advanced features of a commercial code and do not intend to develop a complete new code.

Equation 1 has the same form as that for heat conduction. The analogies between these two processes[15] (mole fraction needs to be interpreted as temperature and mass diffusion coefficient as thermal conductivity; mass density and the specific heat at constant pressure can be set equal to one) are the reason why the heat transfer module of a commercial finite element code can be used to solve the partial differential equation according to Eq 1. The finite element discretization of Eq 1 yields the following backward finite difference scheme for the time step $k + 1$:

$$\left(\frac{\boldsymbol{C}}{\Delta t} + \boldsymbol{K}\right)\boldsymbol{T}^{k+1} = \left(\frac{\boldsymbol{C}}{\Delta t}\right)\boldsymbol{T}^{k} + \boldsymbol{Q} \qquad \text{(Eq 3)}$$

where $\boldsymbol{C}$ is the capacity matrix, $\boldsymbol{K}$ the diffusivity matrix, and $\boldsymbol{Q}$ the vector of nodal loads. Vector $\boldsymbol{T}$ contains the nodal oxygen mole fractions. In a transient linear mass diffusion analysis, the diffusivity matrix $\boldsymbol{K}$ is a constant and the source expression given in Eq 2 contributes only to the right-hand side of Eq 3. The solution procedure for the coupled system of differential equations is schematically shown in Fig. 2. Standard modules of the code are surrounded by dotted boxes while extensions of the functionality are marked by solid boxes. The vector of nodal oxygen

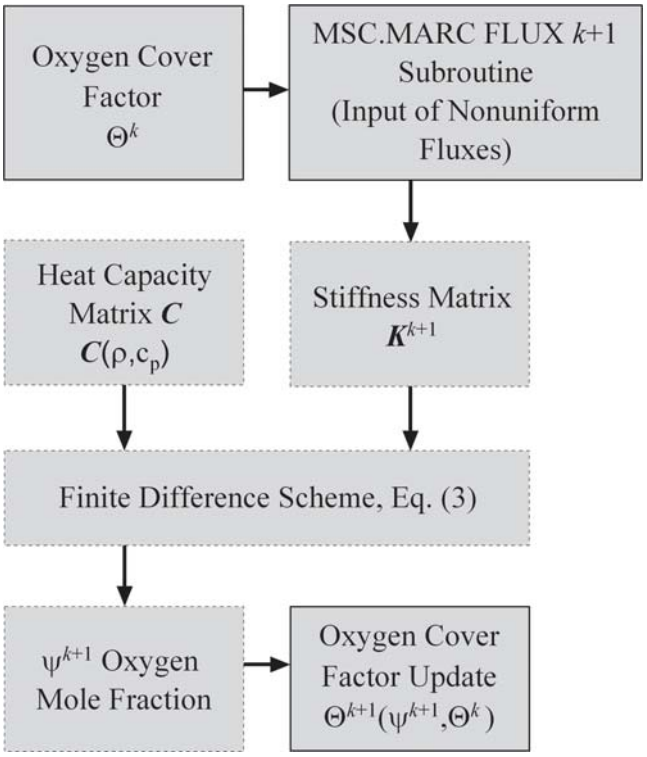

Fig. 2 Extended finite element scheme

mole fractions is obtained for each time increment according to Eq 3. Then, Eq 2 represents for known ψ^{k+1} an ordinary differential equation with respect to Θ. The update of the surface coverage $\Theta^k \rightarrow \Theta^{k+1}$ requires an indirect scheme (internal iteration loop variable: j; n refers to the node number) that incorporates linearization of the right-hand side of Eq 2 to ensure convergence of the solution:

$$\Theta_{n(j+1)}^{k+1} - \Theta_n^k = \Delta t\left[\gamma_O\left(\psi_{O,n}^{k+1}, \Theta_{n(j)}^{k+1}\right) + \frac{\partial}{\partial\Theta}\gamma_O\left(\psi_{O,n}^{k+1}, \Theta_{n(j)}^{k+1}\right)\cdot\left(\Theta_{n(j+1)}^{k+1} - \Theta_{n(j)}^{k+1}\right)\right] \quad \text{(Eq 4)}$$

Iteration of the scheme given in Eq 4 is stopped as soon as the difference of two iteration loops is smaller than a certain tolerance ε, that is, $\Theta_{n(j+1)}^{k+1} - \Theta_{n(j)}^{k+1} < \varepsilon = 0.01$. However, the iteration scheme given in Eq 4 and the complex source expression (Eq 2) is not a standard functionality of a commercial finite element program and has been implemented into the code MSC.Marc due to special user-subroutines (see Fig. 2, dotted boxes).

4. Results

In the examples in this section, the influence of the oxide particle distribution and the oxide shape on the oxygen mole fraction and oxygen surface coverage is investigated for two-dimensional models. For all simulations, the magnesium mole fraction ψ_{Mg} was equal to 0.03 (the Mg mole fraction is used to calculate the *volume* fraction of MgO to estimate the surface A of the oxide in Eq 2[16]), and an oxygen diffusion coefficient of $D_O = 2.72 \times 10^{-2}$ exp $(-46{,}055/(RT))$ mm^2/s was incorporated. Other parameters were assigned as follows: $\alpha = \beta = 1$; $\nu_a = \nu_d = 2 \times 10^7$ s^{-1}; $E_a = 10 \times 10^3$ J/(mol·K), $E_d = 100 \times 10^3$ J/(mol·K), $T = 773$ K, $a = 10^3$ J/mol, $b = 10^4$ J/mol.[16] It should be noted here that the presented examples can easily be extended to three-dimensional problems.

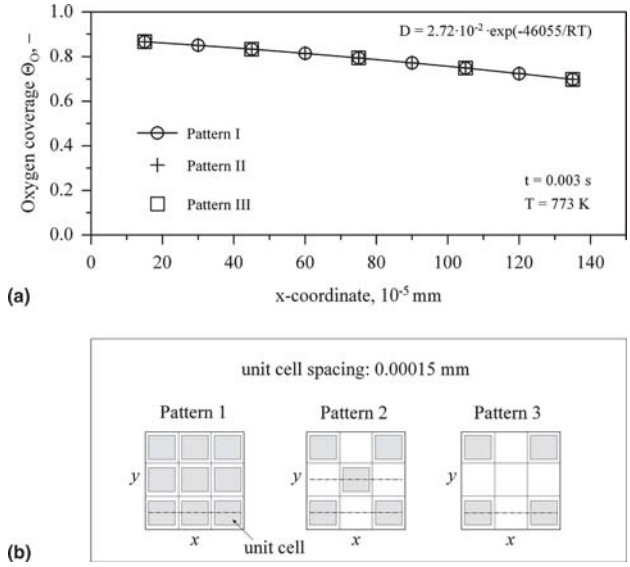

Fig. 3 Distribution of oxygen coverage for periodic particle distribution. Part (b) shows representative unit cells of the oxide arrangement.

4.1 Different Periodic Arrangements of Oxide Particles

In the first example, three different periodic arrangements of oxide particles were considered (Fig. 3b represents unit cells of the different patterns): In the case of distribution I, the oxide particles were modeled as volume sources and equally distributed to *all* finite elements. As a result, each element represents an oxide particle. For patterns II and III, volume sources were only assigned to defined elements in a specific pattern while the sum A of all surface areas of the metal/oxide interfaces was the same for all arrangements. As a result, the power (rate of concentration) of the source for a single element differs from pattern to pattern which was realized by different surface areas of the interfaces. All sources were realized in the finite element code as volume fluxes so that the power of the source was distributed over the entire element volume and not assigned at the nodes of the elements. The results shown in Fig. 3(a) refer to a rectangular specimen with dimensions 0.03 × 0.0015 mm (the coordinate system is situated in the lower-left corner of the rectangle and the bigger dimension is related to the extension along the x-axis). The whole finite element model comprises 2000 elements, which corresponds to 2211 nodes. At the left boundary, a Dirichlet (i.e.,

concentration) boundary condition ψ_O ($x = 0$, $t > 0$) = 0.0005 was prescribed, while the right and horizontal boundaries were isolated (i.e., flux equal to zero). As initial conditions ($t = 0$), oxygen mole fraction and surface coverage were set equal to zero. Figure 3(a) shows the distribution of the surface coverage along certain lines for the different periodic patterns close to the boundary of the specimen. The evaluation paths are indicated in Fig. 3(b) by dash-dot lines. As can be easily seen, there is practically no difference for the surface coverage under the chosen model parameters. However, it should be mentioned that a stronger concentration of the sources in fewer elements, that is, a bigger distance between the sources, can modify the results.

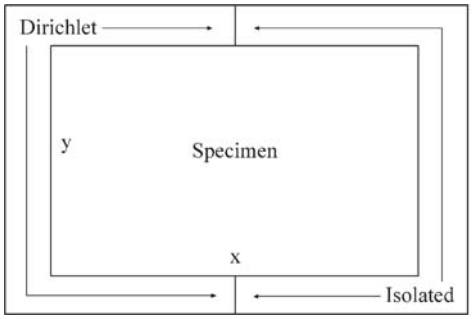

Fig. 4 Principal representation of the boundary conditions

Figure 4 refers to squared specimen (0.012 × 0.012 mm) where 50% of the total boundary was defined as a Dirichlet (ψ_O ($t > 0$) = 0.005) boundary condition, while the remaining part was isolated (flux equal to zero). As initial conditions, oxygen mole fraction and surface coverage were set equal to zero. The growth of the mole fraction and the coverage for two different time steps is shown in Fig. 5(a) and (b) for a source arrangement according to pattern I as shown in Fig. 3(b). A smooth growth of both quantities can be observed for this case of equally distributed oxide particles.

4.2 Agglomeration of Oxide Particles

The next examples consider four different arrangements of oxide particles. Figure 6 illustrates the case of several oxide agglomerations. However, no real shapes of particles were modeled in this example, but the source elements of equal force were concentrated in a nonperiodic way. The size of all elements and thus the size of an oxide particle is equal to 0.00015 × 0.00015 mm. It is obvious that such a distribution is much closer to real particle distributions. Figure 7(a) and (b) highlight the strong influence of such an agglomerated distribution on the oxygen mole fraction and coverage. As can be seen from Fig. 7(a), the oxygen mole fraction reveals a smooth and continuous distribution, while the spatial distribution of the oxygen coverage consists of

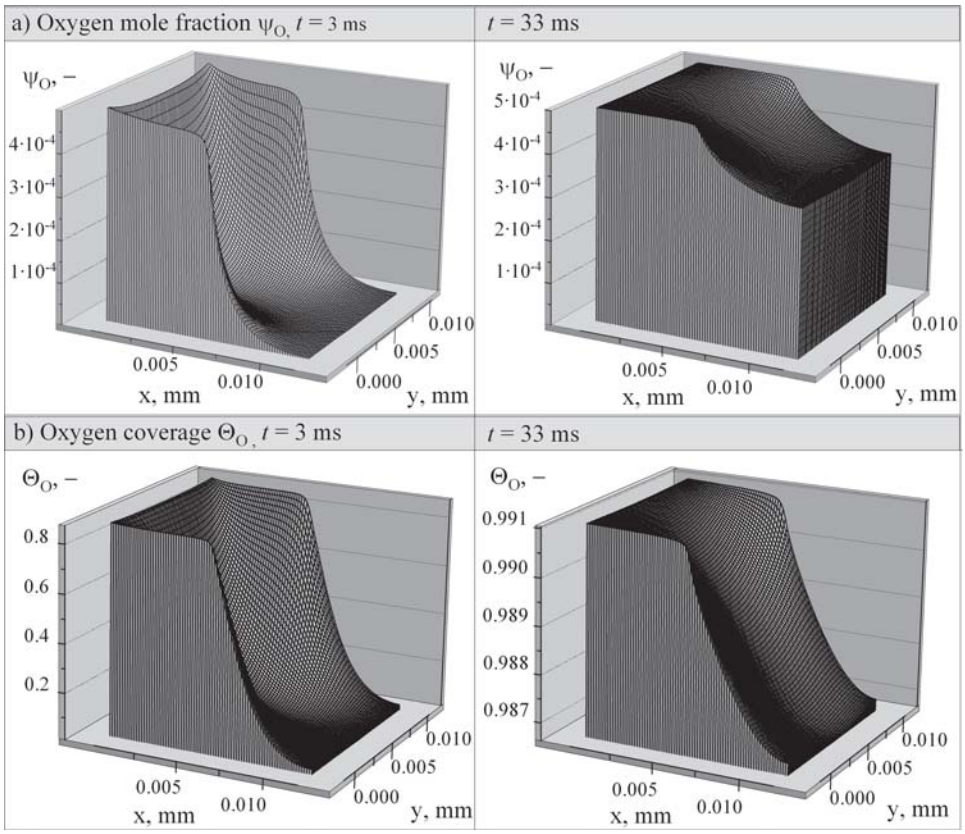

Fig. 5 Evolution of oxygen mole fraction and coverage for different time steps (periodic arrangement, boundary conditions according to Fig. 4)

single values. For this simulation, the initial coverage was set equal to 0.9 and the specimen (0.012 × 0.012 mm) boundary was completely isolated (flux equal to zero). As a result, oxygen coverage is decreasing with time while the mole fraction increases. The final example in this section compares three different random oxide distributions, cf. Figure 8. As can be seen from Fig. 8(a), the particles are slightly more concentrated at the left boundary while the second distribution is slightly more concentrated in the middle and the third more to the right boundary. Additionally, the surface of a single oxide particle (material parameter) A differs for each case (A_1:A_2:A_3 = 1:2:1.333) while the sum A times number of source elements m remains constant. The initial values for mole fraction and coverage were equal to zero and a constant concentration (ψ_O ($t > 0$) = 0.005) was assigned to the left boundary ($x = 0$) while the remaining boundary was isolated. The total sum of the oxide surfaces was again constant for all distributions. As can be seen in Fig. 9, the time evolution of the oxygen coverage sum shows for these three different distributions a significant influence on the particle distribution, while the steady-state value remains the same for all three cases.

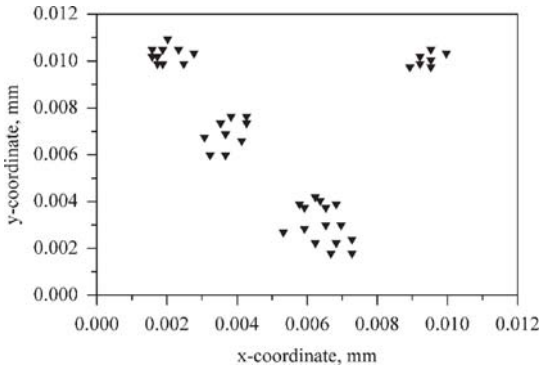

Fig. 6 Positions of oxide particles for random arrangement

4.3 Consideration of the Particle Shape

The final example presents the realistic incorporation of the particle shape. As an example, a single elliptic-shaped oxide particle was modeled (see Fig. 10b inset) embedded in uniform base materials. In this case, only the elements of the particle boundary layer act as the interface between the base materials and oxide particle. For simplicity, the diffusion of oxygen atoms along the particle surface was assumed to be negligible in the computational study. As in the previous example, the initial values for mole fraction and coverage were equal to zero and a constant concentration (ψ_O ($t > 0$) = 0.005) was assigned to the left boundary ($x = 0$) while the remaining boundary was isolated. This type of approach is quite extensive, but allows for the spatial differentiation of the mole fraction and oxygen coverage along the particle surface. Figure 10 illustrates the variation of both quantities

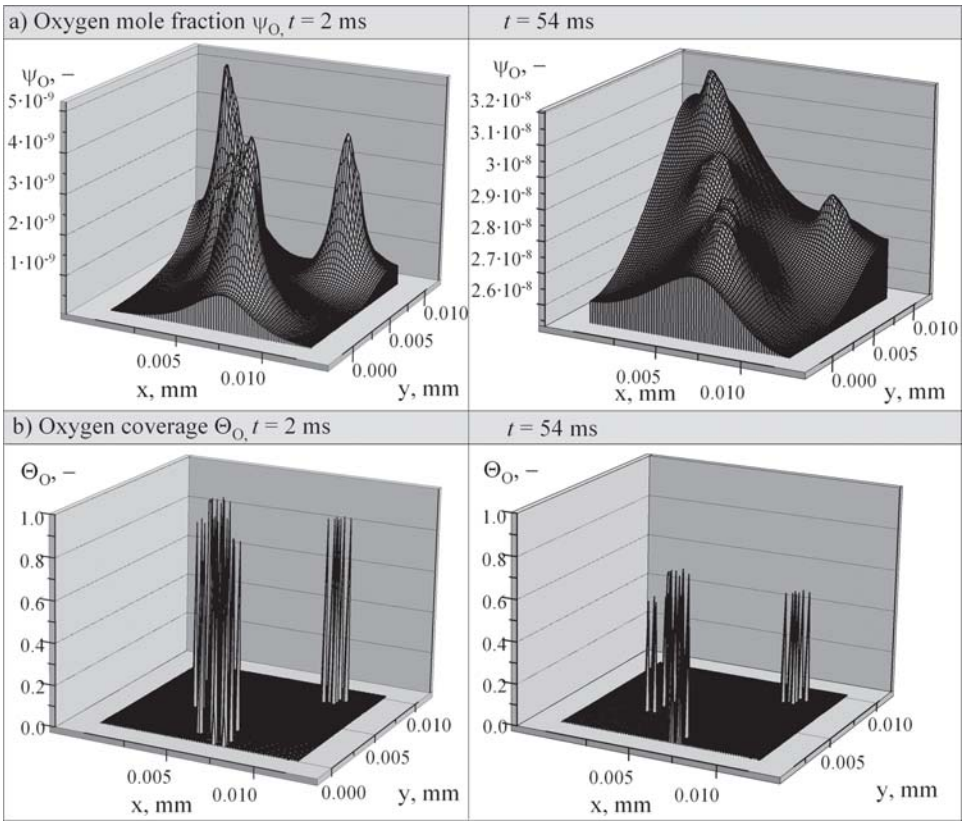

Fig. 7 Evolution of oxygen mole fraction and coverage for different time steps (random arrangement)

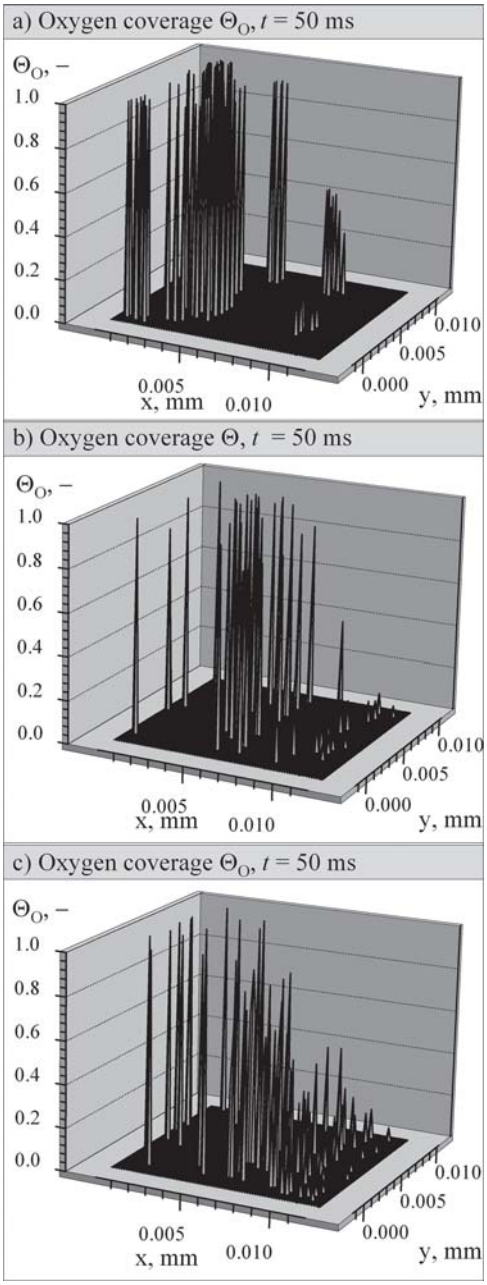

Fig. 8 Oxygen coverage distribution for different stochastic oxide distributions

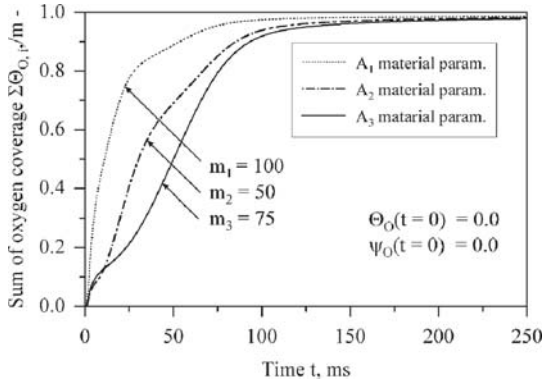

Fig. 9 Variation of the sum of the oxygen coverage with time for different stochastic oxide distributions

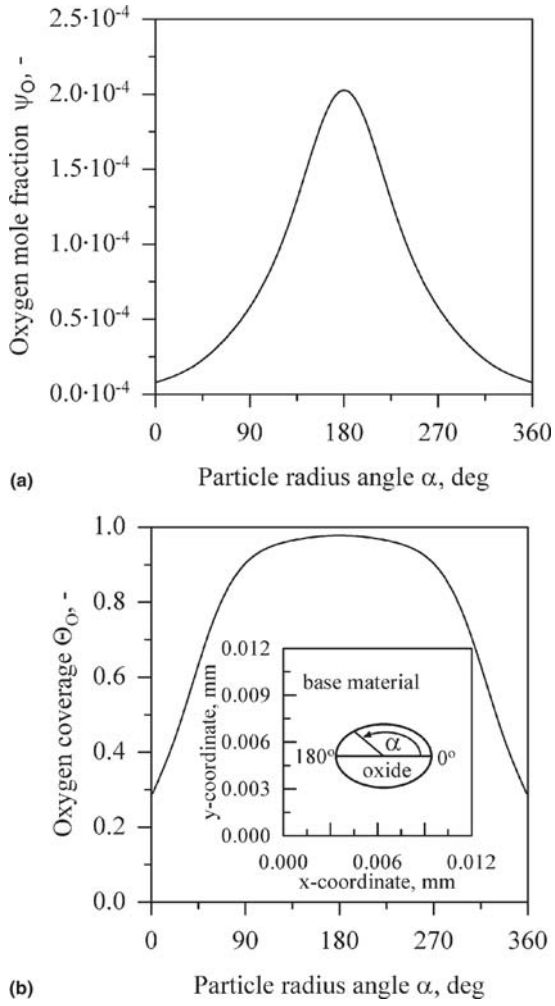

Fig. 10 Oxygen mole fraction and surface coverage along the surface of an elliptic oxide particle

along the oxide surface. As can be seen, the segments of the oxide surface that are facing the specimen boundary are exposed to higher values of the mole fraction and coverage. On the opposite side of the particle, both values are much smaller since the particle shields this segment of its own surface.

5. Discussion and Outlook

A commercial finite element has been extended due to user subroutines to solve a coupled system of partial differential equations, which describes the segregation of oxygen at metal/oxide interfaces. Different modeling approaches for the distribution (i.e., periodic or agglomerated) and for the shape (i.e., simplified as a single element or a real shape)

have been investigated, and it could be shown that the type of distribution clearly influences the distribution of molar mass and surface coverage. Since the presented approach is based on a commercial finite element code, real particle distributions, for example, stemming from image processing software, can be incorporated into numerical simulation. Consideration of the real spatial extension of oxide particles can give rise to further interesting numerical simulations that may be used to investigate, for example, the shielding of particles among each other or to model the spatial distribution of mechanical and physical properties within a specimen and at the interfaces.

Acknowledgment

The authors are grateful to Portuguese Foundation of Science and Technology for financial support.

References

1. A. Gonis and P. Tuchi, *Stability of Materials. Structure-Property Relationship of Metal-Ceramic Interfaces,* Gordon & Breach, 1996
2. E. Pippel, J. Woltersdorf, J. Gegner, and R. Kirchheim, Evidence of Oxygen Segregation at Ag/MgO Interfaces, *Acta Mater.,* 2000, **48,** p 2571-2578
3. J. Gegner and A. Weible, Internal Oxidation of Palladium-Magnesium Alloys, *Z. Metallkd.,* 2000, **91**(12), p 1026-1029
4. R.A. Rapp, The Transition from Internal to External Oxidation and the Formation of Interruption Bands in Silver-Indium Alloys, *Acta Metall.,* 1961, **9,** p 730-741
5. G. Böhm and M. Kahlweit, Über die innere Oxidation von Metallegierungen, *Acta Met,* 1964, **12**(1), p 641-648, in German
6. V.A. van Rooijen, E.W. van Royen, J. Vrijen, and S. Radelaar, On Liesegang Bands in Internally Oxidized AgCd-Based Ternary Alloys, *Acta Metall.,* 1975, **23,** p 987-995
7. D. Stöckel and H.J. Grabke, Die Innere Oxidation von Silberlegierungen bei hohem Druck und in atomarem Sauerstoff, *Z. Metallkd.,* 1973, **64**(4), p 286-295, in German
8. D. Wolf and S. Yip, *Materials Interfaces,* Chapman & Hall, UK, 1992
9. M. Stasiek, A. Öchsner, and J. Grácio, Segregation of Oxygen at Metal/Oxide-Interfaces: Effect of Kinetics and Precipitate Distribution, *Proc. First' International Conference on Diffusion in Solid and Liquids DSL-2005,* July 6-8, 2005, A. Öchsner, J. Grácio, and F. Barlat, Ed., University of Aveiro, Aveiro, Portugal, p 723-726
10. A. Öchsner, M. Stasiek, and J. Grácio, Ad- and Desorption of Oxygen at Metal-Oxide Interfaces: Numerical Approach for Non-Homogeneous Oxide Distribution, *Defect Diffus. Forum,* 2006, **249,** p 35-40
11. A. Öchsner, J. Gegner, and J. Grácio, Quantitative Determination of Microstructural Inhomogeneity for Directional Particle Distribution, *Prakt. Metallogr,* 2005, **42**(33), p 116-125
12. C. Giovanardi, A. di Bona, T.S. Moia, S. Valeri, C. Pisani, M. Sgroi, and M. Busso, Experimental and Theoretical Study of the MgO/Ag(001) Interface, *Surf. Sci.,* 2002, **505,** p L209-L214
13. C. Aharoni and F.C. Tompkins, Kinetics of Adsorption and Desorption and the Elovich Equation, *Advanc. Catalysis,* 1970, **21,** p 1-49
14. F.C. Tompkins, *Chemisorption of Gases on Metals,* Academis Press, London, UK, 1978
15. G.K. Batchelor, *Introduction to Fluid Dynamics,* Cambridge University Press, UK, 1967
16. J. Gegner, "Segregation of Oxygen at Metal/Oxide Interfaces," Ph.D. Thesis, University of Stuttgart, Germany, 1995